

# Relation between structure and mechanical properties (elastoplastic and fracture behavior) of hybrid organic–inorganic coating

A. Ferchichi · S. Calas-Etienne · M. Smaïhi ·  
G. Prévot · P. Solignac · P. Etienne

Received: 21 December 2008 / Accepted: 17 February 2009 / Published online: 6 March 2009  
© Springer Science+Business Media, LLC 2009

**Abstract** The mechanical properties of various inorganic organic films were studied and compared in order to investigate the relation between structural modifications and the mechanical behavior. Films were prepared by a sol–gel process and spin-coated on silicon substrate. The organic–inorganic hybrid is composed of a mixture of colloidal silica and organosiloxane precursors. The functionality of the organosiloxane and the nature of its organic part have been modified to obtain a structural change. Mechanical properties were studied using nanoindentation. Analysis of the strength evolution as a function of depth of indentation shows the layer hardness and elastic modulus. Moreover, coating and interface toughness and residual stresses were determined by a time resolved study of energy dissipation during indentation. The structural changes were determined using liquid and solid  $^{29}\text{Si}$  NMR spectroscopy. Quantity of partially and fully condensed species in the deposited sol and final solid are discussed in relation to the mechanical properties.

## Introduction

Since few years, organic–inorganic hybrid materials based on a mineral network issued from the sol–gel process and

an organic polymerized part are more and more intensively studied. They offer a very innovative way to develop a wide variety of new materials because of their structure at the nanometer scale which combines the properties of an organic and an inorganic entity.

For an industrial point of view, these materials are much more used as layer forms such as protective coatings [1], materials with high transparency [2], transistors [3], luminescent diodes [4], solar cells [5], waveguides [6] and photochromic coatings [7].

In all processes where coatings are used, the ability to have a crack-free system depends on the mechanical properties both of the layer and the interface versus the substrate. In such a case, coating and interface toughness are the properties that will play a major role in the “life or death” of the system. Those properties depend obviously on the composition and on the structure at nanometer scale.

The aim of this paper is to have a better understanding of such a problem by studying a reference material issued from a sol where slight and controlled composition change induces a little structure variation. Such a sol is a mixture of colloidal silica and an organosiloxane precursor ( $\text{R}_n\text{Si}(\text{OR}')_{3-n}$ ). The structural changes are performed by modification of the functionality ( $n$ ) and/or of the non-polymerizable organic group nature (R). The mechanical properties are studied using the well-known nanoindentation technique [8]. Analysis of the force as a function of the indentation depth gives the hardness and the elastic modulus of the coating. When cracks appear, another calculus based on even the crack length (geometric approach) or the dissipative work involved (energetic approach) allows determination of the coating and interface toughness [9, 10]. Note that the geometric approach also allows the measurement of the residual stresses [9, 10]. To analyze the structure and to understand the connection of the different

A. Ferchichi · S. Calas-Etienne (✉) · P. Solignac · P. Etienne  
Groupe d’Etude des Semiconducteurs, Université Montpellier 2,  
Place E. Bataillon, 34095 Montpellier, France  
e-mail: scalas@univ-montp2.fr

M. Smaïhi  
Institut Européen des Membranes, CNRS, Route de Mende,  
34293 Montpellier, France

G. Prévot  
LCVN Université Montpellier 2, Place E. Bataillon,  
34095 Montpellier, France

atoms in the material network, we have chosen the <sup>29</sup>Si NMR spectroscopy at a liquid state for the sols and at the solid one for the coatings [11, 12].

### Experimental procedure

#### Sol synthesis and layers coatings

Each sol is composed of an alcoholic solution of colloidal silica particles (13 nm diameter) and an organosiloxane precursor, R<sub>n</sub>Si(OR')<sub>3-n</sub>. The functionality effect is studied using the dimethyldiethoxysilane (n = 2) and the methyltriethoxysilane (n = 1). R group is methyl or phenyl group in order to study the effect of steric hindrance. Each organosiloxane precursor is mixed to colloidal silica and hydrolyzed with a 0.1 N aqueous hydrochloric solution. The sol was stirred for 24 h at room temperature. The hybrid composition is maintained to 70% mass of colloidal silica and 30% mass of organosiloxane.

Sols are spin-coated with free evaporation at 1200 rpm for 15 s on silicon substrates. This step is followed by a drying and densification step using an adapted thermal treatment. Thermogravimetric analysis has been done to optimize the thermal treatment in order to obtain a crack-free and most densified coating with a safe organic part.

#### Mechanical characterization

The mechanical properties are obtained using the nanoindentation technique. The force required to indent a material is monitored as a function of the depth. In our case, we used a home-made apparatus having a Berkovich indenter, an indentation range from 50 nm to 10 μm at a speed ranging from 0.1 μm/min to a few μm/min, and a maximal force value of 1 N. Surface before and after each experiment can be observed with an integrated optical microscope.

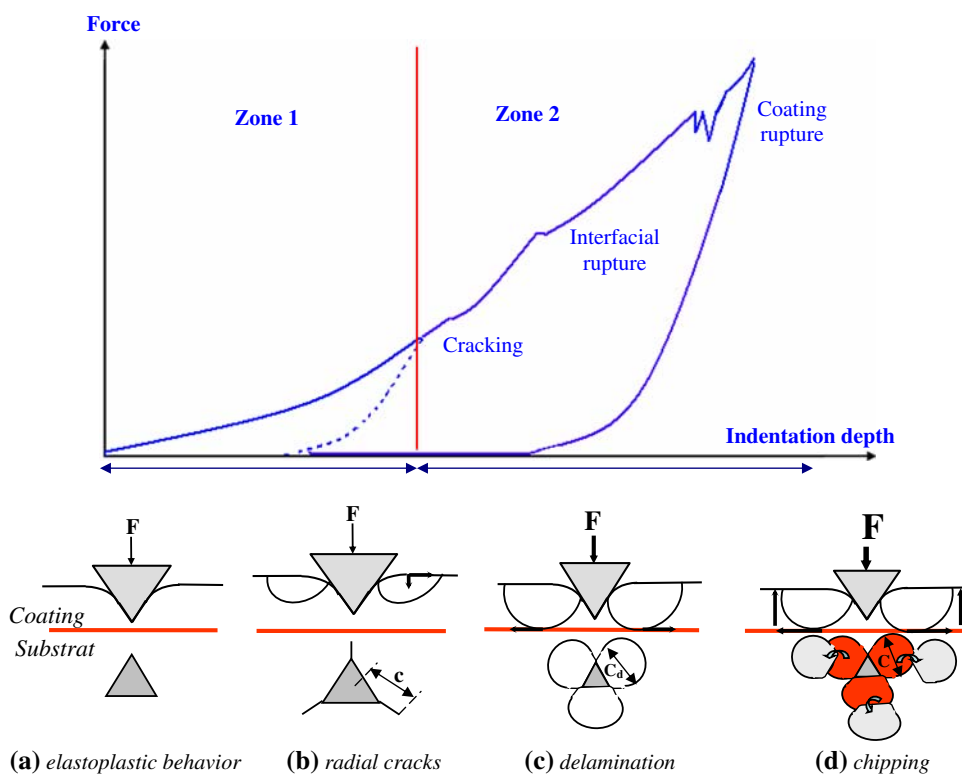
During an indentation experiment, several zones appear on the force versus indentation depth curve (Fig. 1), which are characteristics to the peculiar behavior of the coating. In the zone 1, the indenter is penetrating the material according to its elastoplastic properties such as hardness, H<sub>C</sub>, and elastic modulus, E<sub>C</sub> (Fig. 1a). Hardness is defined as the ratio between the maximum force, F<sub>max</sub>, and the contact area, A, just before the unloading part of the curve [13, 14].

$$H_C = \frac{F_{max}}{A} \tag{1}$$

A is obtained thanks to a previously described calibration procedure [10].

The elastic modulus is calculated using the unloading part of the curve:

**Fig. 1** Indentation curve and different cracking steps



$$E_C = \frac{\frac{\sqrt{\pi}S}{2\sqrt{A}} E_i (1 - \nu_c^2)}{E_i - \frac{\sqrt{\pi}S}{2\sqrt{A}} (1 - \nu_i^2)} \quad (2)$$

where  $S$  is the slope of the linear zone at the beginning of the unloading,  $E_i$  is the elastic modulus of indenter,  $\nu_i$  and  $\nu_c$  are the Poisson coefficients, respectively, of indenter and coating.

At higher indentation depth, the coating can crack. This phenomenon is instantaneously monitored on the force versus indentation curve (zone 2). Three successive steps can be observed (Fig. 1b–d). First, radial cracks occur originating from the edges of the indenter (Fig. 1b). The initiation and the propagation of these cracks depend both on the toughness of the coating,  $K_{IC}$ , and on the residual stresses,  $\sigma_c$ . Theoretical calculus shows a relationship between such properties and the crack length,  $c$ , and the applied force,  $F_{max}$  [15].

$$K_{IC} = 0.016 \left( \frac{E_C}{H_C} \right)^{1/2} \frac{F_{max}}{c^{3/2}} + Z\sigma c^{1/2} \quad (3)$$

where  $Z$  is a geometric factor defined by Broek [15] depending on the indentation depth and the length of the crack.

Making experiments at different maximal force values allows to draw the linear curve  $F_{max}/c^{3/2}$  versus  $c^{1/2}$ . The slope gives  $\sigma_c$ , and the intercept at zero crack length value gives  $K_{IC}$ .  $E_C$  and  $H_C$  have to be previously calculated with an experiment involving no cracks.

Secondly, when the cracks reach the substrate, they get curved and propagate at the interface forming the delamination zone (Fig. 1c). The stress field makes that the area appearing from one corner to another is quite circular with a mean diameter value  $C_d$ . In this case, two methods can perform the  $K_{IC}$  calculus. The first one, called “geometric method”, is based on the  $C_d$  measurement at  $F_{max}$  using the following relationship [9, 16]:

$$K_{int} = \frac{0.792 H_C \sqrt{(1 - \nu_c^2) e}}{[1 + \nu_c + 2(1 - \nu_c) H_C C_d^2 / F_{max}]} \quad (4)$$

The second approach, called “energetic method”, uses the dissipated energy,  $U_d$ , during the indentation experiment [9, 10, 16, 17]:

$$K_{int} = \sqrt{E_{int} \frac{U_d}{\pi C_d^2}} \quad (5)$$

where  $E_{int}$  is the composite modulus between the coating ( $E_c$ ) and the substrate ( $E_s$ ) [18].

$$\frac{1}{E_{int}} = \frac{1}{2} \left( \frac{1}{E_c} + \frac{1}{E_s} \right) \quad (6)$$

Finally, at highest force values, these cracks get curved again to go up to the coating surface and segments of the

coating are taken off, marking the chipping phase (Fig. 1d). The energy required to crack the coating,  $U_c$ , gives another possibility to calculate the coating toughness using the following relationship [19, 20]

$$K_{IC} = \sqrt{\frac{E_C U_c}{3 \pi e' C_c}} \quad (7)$$

where  $e'$  is the efficient thickness of the coating which is higher than real thickness  $e$ , because cracks are not perpendicular to the surface.  $C_c$  is the diameter of the chipping disc.

## <sup>29</sup>Si NMR characterization

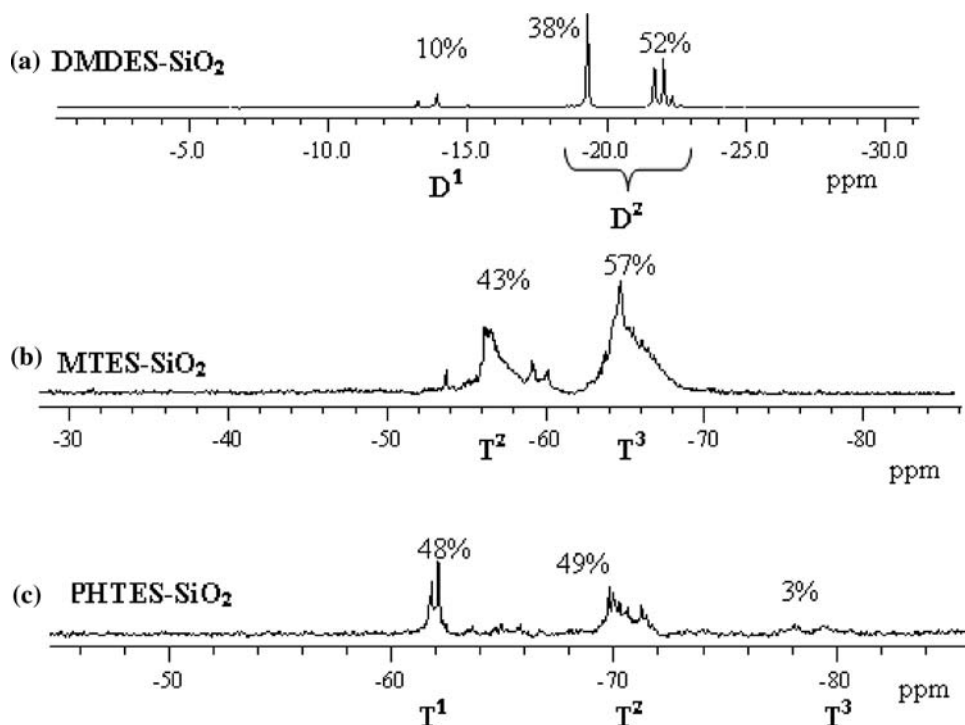
<sup>29</sup>Si NMR spectroscopy is a very useful technique to differentiate the silicon atom as a function of their neighbors. As already referenced in the literature, condensed species will be noted  $D^n$ ,  $T^n$  and  $Q^n$  for dialkyl, trialkyl and tetraalkyl precursors, respectively.  $n$  represents the number of bridging oxygen [11]. These species can be partially or totally condensed and for some cases cyclic species can also be formed [12].

To better understand the material structure, we made experiments in the liquid state for the sols and in the solid state after the thermal treatment. For all the sols, liquid <sup>29</sup>Si NMR spectra were obtained using Bruker Avance 300 MHz spectrometer. Glass tubes were used for this analysis. For this reason it was not possible to analyze the tetrafunctional peak zone corresponding to Q species. <sup>29</sup>Si NMR CP MAS solid-state spectra were recorded on an ASX400 Bruker spectrometer (79.49). However, it was impossible to perform such a measurement on coated samples because of lack of solid. We decided to elaborate bulk samples in conditions as close as possible to those of the coatings. The spin-coating technique used with pure mineral sols is known to cause a higher evaporation rate during the movement of the sample, related to a structural rearrangement due to the shearing strength and inducing denser system [21]. Moreover, previous experiments on hybrids materials showed that the refractive index, a macroscopic picture of the structure, did not change under spin-coating conditions. This result was explained by the lower reactivity of hybrid precursors compared to pure mineral ones [22]. So, to be close to the deposition conditions, the sol was simply spread out in large dugs with only 1–2 mm thickness. Drying was then performed under an air flow to enhance the natural evaporation.

## Results

Liquid <sup>29</sup>Si NMR spectra are presented in Fig. 2. They put in evidence the different condensed species content in the sol before deposition. All the positions of peaks are identified by comparison with literature data [11, 12, 23–25].

**Fig. 2** Liquid  $^{29}\text{Si}$  NMR spectra for the different systems



DMDES-SiO<sub>2</sub> system (Fig. 2a) has three peaks domains. The first one located around  $-14$  ppm is attributed to D<sup>1</sup> species. The other ones correspond to two kinds of D<sup>2</sup> species. The thin peak located at  $-19.2$  ppm is assigned to a cyclic arrangement of four siloxanes bonds, called D<sup>2</sup><sub>4c</sub> [25] while the peak around  $-22$  ppm corresponds to linear oligomers. D<sup>2</sup> ratio of 90% indicates a high condensation state. MTES-SiO<sub>2</sub> system (Fig. 2b) has also two peaks domains. T<sup>1</sup> species are not detected and only T<sup>2</sup> and T<sup>3</sup> species are put in evidence around  $-57$  and  $-65$  ppm respectively. Fully condensed species quantity is about 57%. On the other hand, when MTES is replaced by PHTES (Fig. 2c), a large part of T<sup>1</sup> and T<sup>2</sup> species appear on the spectrum with only 3% of T<sup>3</sup> species. The sol is less condensed than the first systems.

Solid  $^{29}\text{Si}$  NMR spectra are represented in Fig. 3. Two main groups of bands appear. The first one corresponds to silicon atoms of the organosiloxane part of the system while the other represents the silicon atoms of the silica particles. As four siloxane bonds are possible, such species are called Q<sup>n</sup>. A spectral decomposition is necessary to separate different species contributions and to calculate their respective quantity. Results are listed in Tables 1 and 2. DMDES-SiO<sub>2</sub> system (Fig. 3a) shows two D<sup>2</sup> peaks corresponding to D<sup>2</sup><sub>4c</sub> and linear D<sup>2</sup> species around  $-19$  and  $-22$  ppm respectively. D<sup>1</sup> species are not detected in the solid state. Moreover, more D<sup>2</sup><sub>4c</sub> species are present compared to the liquid state (61% against 38%). MTES-SiO<sub>2</sub> system (Fig. 3b) shows two T peaks domains assigned to T<sup>2</sup> and T<sup>3</sup> species around  $-57$  and  $-65$  ppm

respectively. T<sup>3</sup> quantity about 81% involves an important condensation state of the solid. On the other hand, PHTES-SiO<sub>2</sub> system (Fig. 3c) does not show the same behavior as at the liquid state. The condensed species undergo an important increase during the thermal treatment to reach a quantity close to MTES-SiO<sub>2</sub> system.

To give an example of mechanical measurements, nanoindentation curve and imprints pictures for MTES-SiO<sub>2</sub> system are represented in Fig. 4. Mechanical properties were calculated using both the geometric and the energetic methods. Figure 5 shows the example of such a calculation for the MTES-SiO<sub>2</sub> system. The method is the same for the other ones. All results are listed in Table 3. Coating toughness values, obtained using the geometric method, are lower than using the energetic one. The MTES-SiO<sub>2</sub> system has the best mechanical properties and the highest residual stresses while the DMDES-SiO<sub>2</sub> system has the lowest ones. The PHTES-SiO<sub>2</sub> system is in an intermediate state.

## Discussion

MTES-SiO<sub>2</sub> system has the highest mechanical properties. NMR experiments show an important quantity of condensed species at the liquid state (57%), which increases at the solid state (81%), leading to a very condensed structure. Moreover, solid NMR spectra show that Q<sup>3</sup> species exist in a very low quantity. Such a species are normally present at the silica particles surface. These two results indicate that

**Fig. 3** Solid  $^{29}\text{Si}$  NMR spectra for the different systems

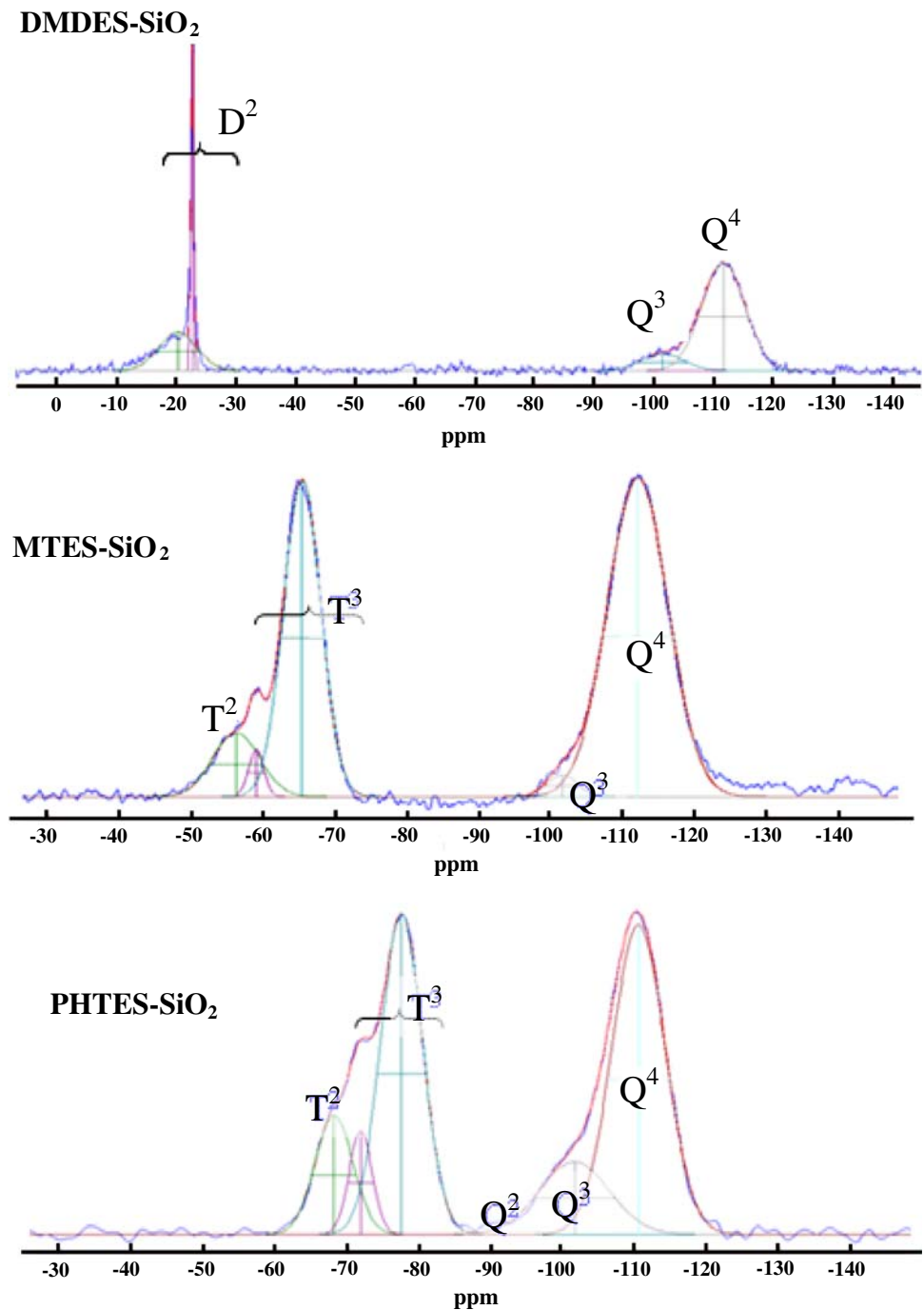


**Table 1** Percentage of the three-functional precursor systems species

System	% T		% Q		
	% T <sup>2</sup>	% T <sup>3</sup>	% Q <sup>2</sup>	% Q <sup>3</sup>	% Q <sup>4</sup>
MTES-SiO <sub>2</sub>	19	81	–	4	96
PHTES-SiO <sub>2</sub>	20	80	3	23	74

silanol groups issued from the hydrolysis of the MTES precursor are very reactive to condense and form siloxane bonds. They react with themselves and with silanol groups

**Table 2** Percentage of the DMDES-SiO<sub>2</sub> system species

System	% D		% Q	
	% D <sup>2</sup> <sub>4c</sub>	% D <sup>2</sup>	% Q <sup>3</sup>	% Q <sup>4</sup>
DMDES-SiO <sub>2</sub>	61	15	4	85

localized at the silica particles surface. The interface toughness value near the value of silica indicates that they react with silanol groups naturally present on the silicon

**Fig. 4** Nanoindentation curve and imprints photos for the MTES-SiO<sub>2</sub> system

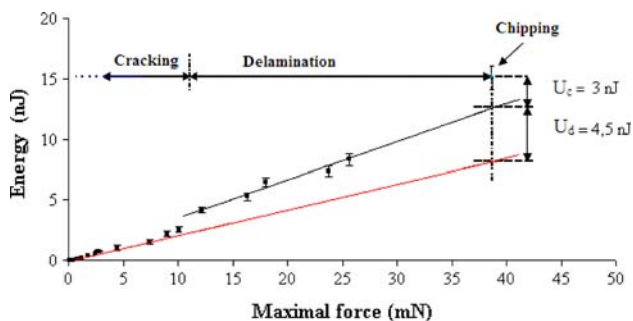
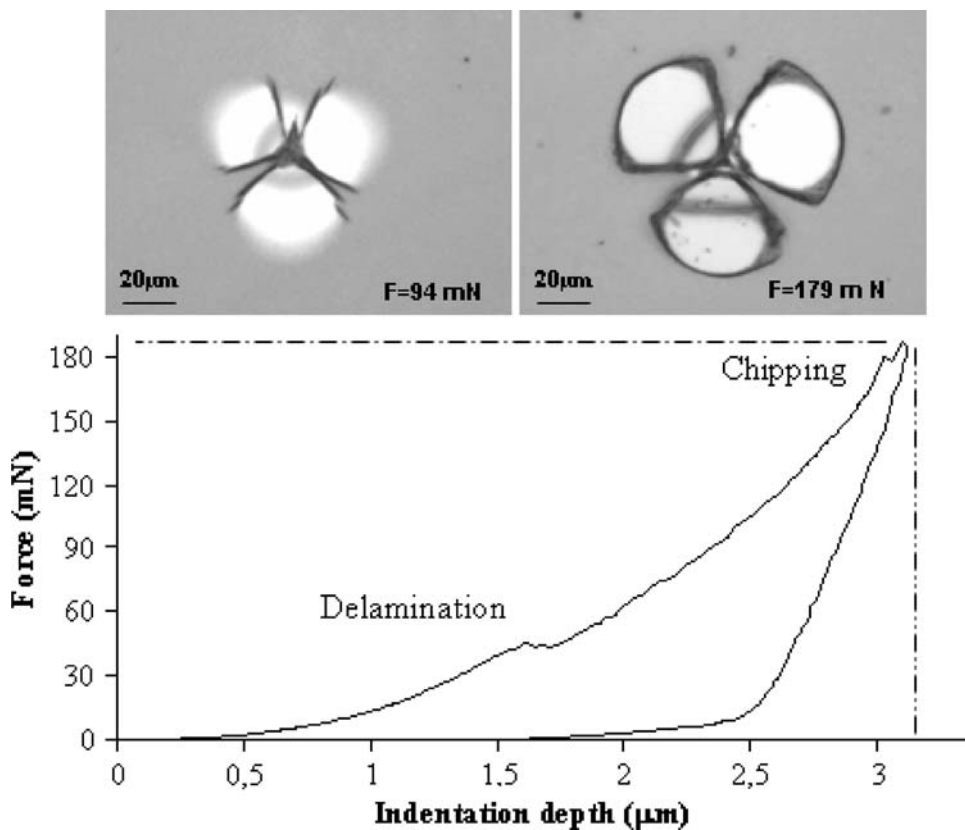


**Fig. 5** Irreversible energy vs. the maximal force for the DMDES-SiO<sub>2</sub> system

substrate. As a consequence, the MTES-SiO<sub>2</sub> system has a very reticulated structure involving mechanical properties which tend to silica ones. High residual stress value is then

due to the important shrinkage involved in the formation of siloxane bonds during the thermal treatment.

If MTES is replaced by DMDES, mechanical properties decrease drastically. The DMDES-SiO<sub>2</sub> system is difunctional, so it would have lower mechanical properties than MTES-SiO<sub>2</sub> system which is trifunctional. NMR experiments are in perfect agreement with this assumption but give additional interesting data. DMDES-SiO<sub>2</sub> system is very condensed but with a large quantity of cyclic species (61% in the solid state). Obviously, they do not take part to the system reticulation [24]. We can conclude that this system is very condensed but poorly reticulated and as a consequence contributes to decrease the mechanical properties. Q<sup>3</sup> species are in a quantity close to MTES-SiO<sub>2</sub> system while Q<sup>4</sup> ones are slightly lower. It indicates that DMDES is less linked to silica particles and it is in

**Table 3** Mechanical properties of the different systems

System	$E_c$ (GPa)	$H_c$ (GPa)	$K_{IC}$ (MPa m <sup>1/2</sup> ) Energetic method	$K_{int}$ (MPa m <sup>1/2</sup> ) Geometric method	$\sigma_r$ (MPa)
DMDES-SiO <sub>2</sub>	2.7 ± 0.1	0.16 ± 0.04	0.07 ± 0.01	0.09 ± 0.01	13 ± 4
MTES-SiO <sub>2</sub>	18.3 ± 0.9	1.41 ± 0.1	0.32 ± 0.05	0.48 ± 0.06	30 ± 7
PHTES-SiO <sub>2</sub>	6.3 ± 0.4	0.27 ± 0.04	0.09 ± 0.01	0.10 ± 0.01	23 ± 6



accordance with the mechanical properties decrease. Concerning the interfacial toughness, we can link the quantity of partially condensed species in the liquid state to the adhesion properties. In fact, partially condensed species give an idea of the possibility of sol attachment to the surface of the substrate. Therefore, the small quantity of partially condensed species  $D^1$  (10%), compared to the 43% of  $T^2$  for the system containing the three-functional precursor in the final sol explain the better adherence on silicon substrate for the MTES-SiO<sub>2</sub> system. Finally, the less important residual stresses in the DMDES-SiO<sub>2</sub> film are the result of the poor adhesion (fewer anchoring points) and the poorer elastoplastic properties.

The second part of this work concerns the effect of the nature of the non-polymerizable organic groups. It is well known that the rate of hydrolysis and condensation reactions decreases when the organic group size increases [26]. Mechanical properties follow the same way. NMR results show a large quantity of partially condensed species and also small quantities of  $Q^2$  species which do not appear in the case of the MTES-SiO<sub>2</sub> system. These not completely condensed species give proof of the low condensation state of the final solid and as a result poor mechanical properties. Concerning the adhesion properties, liquid NMR spectra show a large quantity of partially condensed species in the final sol for the PHTES-SiO<sub>2</sub> systems. Nevertheless, the interfacial toughness values are much lower than those of the MTES-SiO<sub>2</sub> system containing a lower quantity of partially condensed species. These results can be explained by the organic group hindrance during the substitution mechanism which controls the anchoring reaction on silicon surface. For this reason, even if the possibility of linking the surface is high, PHTES-SiO<sub>2</sub> systems have a low adherence on silicon substrate. Low elastic properties and low adherence on silicon substrate are the principal reasons for the weak residual stresses on the systems containing bulky groups. We can therefore conclude that voluminous organic groups involve a lower connectivity and a decrease of mechanical properties but they contribute to the weak residual stresses on the film.

## Conclusion

The mechanical properties of different hybrid coatings have been investigated using the nanoindentation technique. Results show that the change of the organic part bounded to silicon induces a structural change. By relating mechanical properties to the structure, we conclude that MTES-SiO<sub>2</sub> system, which is trifunctional system, has the

best mechanical properties, due to its well condensed and well reticulated network. The PHTES-SiO<sub>2</sub> system is also a trifunctional one but less condensed and reticulated because of the phenyl groups steric hindrance. It shows the lowest mechanical properties. Concerning the adherence, in addition to the necessity of a large quantity of not completely condensed species in the final sol, it is important that the non-polymerizable organic group does not block the substitution mechanism.

In order to confirm these conclusions on the relation between the structure and the mechanical properties of hybrid coatings, the study must be extended to more complex systems coated on different substrates. Moreover, simulations are in progress to complete these conclusions.

## References

1. Frings S, Meinema HA, Van Nostrum CF, Vander-Linde R (1998) *Prog Org Coat* 33:126
2. Etienne P, Phalippou J, Sempere R (1998) *J Mater Sci* 33:3999. doi:10.1023/A:1004609115560
3. Kagan CR, Mitzi DB, Dimitrakopoulos CD (1999) *Science* 286:945
4. Lee TW, Park O, Yoon J, Kim JJ (2001) *Adv Mater* 3:211
5. Huynh WU, Dittmer JJ, Alivisatos AP (2002) *Science* 295:2425
6. Yoshida M, Prasad PN (1996) *Chem Mater* 8:235
7. Biteau J, Chaput F, Lahlil K, Boilot JP, Tsivgoulis GM, Lehn JM, Darracq B, Marois C, Levy Y (1998) *Chem Mater* 10:1945
8. Etienne-Calas S, Duri A, Etienne P (2004) *J Non-Cryst Solids* 344:60
9. Malzbender J, De With G (2000) *J Non-Cryst Solids* 265:51
10. Ferchichi AK, Etienne-Calas S, Etienne P (2008) *J Non-Cryst Solids* 354:712
11. Glaser RH, Wilkes GL (1989) *J Non-Cryst Solids* 11:373
12. Brunet F (1998) *J Non-Cryst Solids* 231:58
13. Loubet J, Georges JM, Marchesini O, Meille G (1984) *J Tribol* 106:43
14. Oliver WC, Pharr GM (1992) *J Mater Res* 7:1564
15. Broek D (1997) *Elementary engineering fracture and mechanics*. Kluwer Academic, Dordrecht
16. Marshall DB, Lawn BR (1977) *J Am Ceram Soc* 60:86
17. Rosenfeld LG, Ritter JE, Lardner TJ, Lin MR (1990) *J Appl Phys* 67:3291
18. Hutchinson JW, Suo Z (1992) *Adv Appl Mech* 92:63
19. Lawn BR (1993) *Fracture of brittle solids*. Cambridge University Press, London, p 378
20. Li X, Diao D, Bhushan B (1997) *Acta Mater* 45:4453
21. Brinker CJ (1988) *J Non-Cryst Solids* 100:31
22. Bissuel F (1996) Ph.D. thesis, University of Montpellier 2
23. Sugahara Y, Okada S, Kuroda K, Kato C (1992) *J Non-Cryst Solids* 13:925
24. Lux P, Brunet F, Virlet J, Cabane B (1996) *Magn Reson Chem* 34:100
25. De Monredon S (2004) Ph.D. thesis, University Paris VI
26. Osterholz FD, Pohl ER (1992) *Silanes and other coupling agents*. Utrecht, p 119